ACS OMEGA

Article

Cite This: ACS Omega 2019, 4, 13189−13199

http://pubs.acs.org/journal/acsodf

High-Performance Styrene-Butadiene Rubber Nanocomposites Reinforced by Surface-Modified Cellulose Nanofibers

Alex Sinclair,[†] Xiaoyi Zhou,[‡] Siwakorn Tangpong,[†] Dilpreet S. Bajwa,[†] Mohiuddin Quadir,*[,§] and Long Jiang*[,†]

[†]Department of Mechanical Engineering, [‡]Department of Statistics, and [§]Department of Coatings and Polymeric Materials, North Dakota State University, North Dakota State University, Fargo, North Dakota 58108, United States

ABSTRACT: Styrene-butadiene rubber (SBR) is widely used in the tire, footwear, and belt industries. SBR products contain a high content of carbon black, which is hazardous to human health and the environment. The goal of this study is to investigate the potential of using bio-based cellulose nanofibrils (CNFs) as a replacement for carbon black under simulated industrial formula/processing conditions. CNFs were surface-modified using five different reagents to have either −SH or −C═C functional groups grafted onto their surfaces. Vulcanized SBR sheets reinforced with pristine CNFs, and the five functionalized CNFs were prepared and their properties were tested and compared with those of industrial SBR containing carbon black. All the CNFs, pristine or modified, demonstrated higher reinforcing efficiencies (property increase/amount of reinforcement) than carbon black. The modified CNFs showed even higher reinforcing efficiencies than the pristine ones because of the former's better dispersion and stronger interfacial bonding. The −SH and −C═C functional groups reduced the hydrophilicity of CNFs and allowed chemical linkages between CNFs and SBR to be established during vulcanization. Solvent (toluene) resistance of the rubber was also improved after the incorporation of CNFs because of the barrier effect of the nanofibers and the restrained SBR chain mobility. The latter also led to reduced rubber damping. Although CNFs provide much stronger reinforcement than carbon black, going forward, SBR/CNFs/carbon black hybrid nanocomposites can also be developed to offer tailorable property combinations that meet different application requirements.

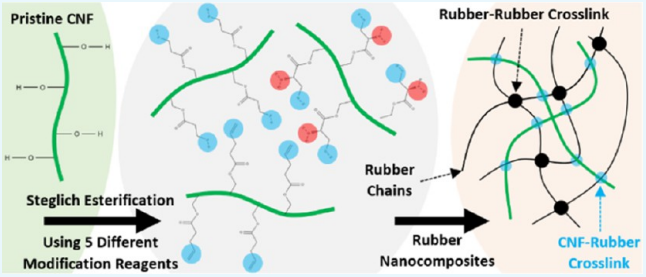

INTRODUCTION

Nanosized reinforcing fillers are commonly incorporated in rubber to increase its strength, abrasion resistance, UV stability, and other performances. The fillers also play a significant role in many aspects of rubber processing, impacting the vulcanization process, curing kinetics, and cross-linking density of the resultant rubber products. The fillers affect the mechanical and viscoelastic properties of rubber through filler−polymer and filler−filler interactions.[1−3] The dominant filler used in the rubber industry is carbon black. Carbon black provides vulcanized rubbers significant improvement in strength as well as resistance to abrasion and UV degradation.[4,5] The weight percentage of carbon black in rubber can be as high as 50%.

There are however many drawbacks involved in both the production of carbon black and its use in rubber. Carbon black is produced through thermal processes using heavy oil or natural gas as the feedstock. In the processes, greenhouse gases and other pollutants are emitted. Carbon black in discarded rubber products such as tires may is potentially harmful if leached into the environment. Carbon black is also a significant workplace safety concern as it is carcinogenic and hazardous. For these reasons, both industry and academia have dedicated resources to develop suitable replacements for carbon black.

In recent years, many nanomaterials have been proposed as potential candidates for rubber reinforcement including: nanoclay, carbon nanotubes, graphene, and cellulose nanofibrils/nanocrystals (CNFs/CNCs).[6−13] CNFs/CNCs represent a unique opportunity as reinforcing fillers for rubbers as these materials are bio-based and their supply is virtually inexhaustible.[14] CNFs/CNCs have a large surface area and a high aspect ratio, which, based on composite mechanics, are ideal for stress transfer and therefore reinforcement. They also feature high strength and modulus and a surface chemical structure which can be tailored to promote strong interfacial bonding to different matrix polymers. The native surfaces of CNFs/CNCs consist of many hydroxyl groups, which are responsible for their strong hydrophilic nature. This poses a challenge in incorporating them into hydrophobic polymers and achieving strong fiber−polymer bonding.[14,15] Surface functionalization of CNFs/CNCs is required in such situations to attach functional groups that can interact with the polymers to the cellulose nanomaterials.

Received: May 7, 2019
Accepted: July 8, 2019
Published: August 1, 2019

DOI: 10.1021/acsomega.9b01313
ACS Omega 2019, 4, 13189−13199

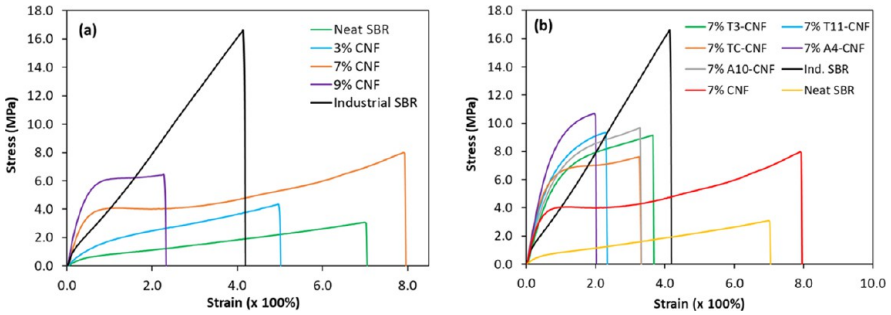

Figure 1. Representative tensile stress−strain curves of SBR nanocomposites reinforced with (a) pristine CNFs and (b) various functionalized CNFs. The curves for the industrial SBR containing 50 phr carbon black and the neat SBR without any carbon black are also shown for comparison.

Trovatti et al. compounded bacterial cellulose (BC) nanofibers and BC decorated with polystyrene (BCPS) into natural rubber (NR) latex for reinforcement.[9] PS was utilized to compatibilize the BC with the hydrophobic NR to improve interfacial adhesion and BC dispersion. The system was vulcanized using sulfur vulcanizing agents. Both BC and BCPS were shown to increase the tensile modulus and strength of the rubber nanocomposites. The storage modulus of the composites mentioned above T_g was significantly increased after incorporating BC or BCPS. Visakh et al. reinforced NR latex with bamboo pulp-derived cellulose nanowhiskers (CNW).[16] A two-step masterbatch technique was used in rubber composite preparation and the rubber was vulcanized using sulfur. The tensile strength was increased from approximately 9 MPa for the neat NR to 14 MPa at 10% CNW. The CNW-reinforced NR also showed higher solvent resistance and higher storage modulus than the neat NR. Yin et al. used BC to reinforce styrene-butadiene rubber (SBR).[17] Tensile strength of the nanocomposites was increased significantly (from 2.4 to 9.9 Mpa) when using up to 2.5 parts per hundred rubber (phr) BC. CNCs were also incorporated into NR, epoxydized NR, and SBR to produce water-responsive nanocomposites. The water-induced, adaptive mechanical behavior was attributed to the establishment/destruction of strong hydrogen bonding between CNCs or between CNCs and rubber chains.[18,19] In all these studies, the rubber latexes were not vulcanized and hence their mechanical properties were relatively low.

Surface functionalization of cellulose nanomaterials has been extensively studied and many important methods have been discussed and summarized in review articles and books.[14,20,21] Parambath Kanoth et al. utilized Fischer esterification to incorporate mercapto functional groups (−SH) onto CNC (m-CNC) and used the material as reinforcement and a cross-linking agent in NR.[22] The free radical thiol−ene cross-linking reactions between m-CNC and NR were initiated by UV irradiation. The nanocomposites containing m-CNC had a higher cross-link density than pristine CNC, indicating the formation of covalent bonds between CNC and the NR matrix. m-CNC-reinforced samples performed significantly better in terms of both tensile strength and strain compared with pristine CNC-reinforced samples. Kato et al. functionalized CNFs by attaching saturated and unsaturated fatty acid chains to the nanofibers via esterification.[23] Both modified CNFs were found to improve the degree of cross-linking of NR and significantly increase its tensile strength and Young's modulus. The CNFs modified with unsaturated fatty acid provided a larger increase in tensile strength because of the additional cross-linking reaction via the C═C of the unsaturated acid.

Rosilo et al. functionalized CNCs via esterification with long-chain unsaturated fatty acids.[24] The functionalized CNCs were incorporated in poly(butadiene) rubber and the composite was cross-linked by UV radiation. TEM results revealed that the CNCs were well dispersed to form intercalated domains of self-aligned CNCs. Tensile strength of the nanocomposites increased with increasing CNC content up to 80%. Chen et al. functionalized cellulose by grafting L-cysteine onto the surface of cellulose fiber.[25] The authors found that this functionalization significantly improved sorption capacity of the fibers toward mercury because of strong affinity between mercury and the thio groups on L-cysteine. L-Cysteine consists of multiple functional groups including amine, thio, and carboxylic acid, which make it potentially versatile for use as a cross-linking agent in many thermosetting polymers.

SBR is the most widely used synthetic rubber in the tire industry.[26] Our literature review has shown that reinforcing SBR via incorporating cellulose nanofibers is still rare. This is especially the case when the vulcanized SBR is intended for tire use (instead of SBR latex for coating and bonding) and functionalized cellulose nanofibers are involved. Therefore, the goal of this research is to systematically study the reinforcement of a series of pristine and functionalized CNFs to SBR products fabricated by the standard rubber production method. The properties of the SBR/CNF nanocomposites will be compared with those of industrial standard SBR that contains 50 phr carbon black. This study showed that CNFs even in their pristine form were much more effective in reinforcing SBR than carbon black. Functionalization of CNFs further increased the level of reinforcement because of their improved dispersion and enhanced interfacial bonding to SBR. Considering other rubber properties offered by carbon black including UV resistance, electrical/thermal conductivities, and so forth, a CNFs/carbon black/SBR hybrid nanocomposite should also be considered to achieve a property set that is comparable to or better than that of carbon black-filled traditional SBR products.

RESULTS AND DISCUSSION

Tensile Properties. Mechanical properties of the various SBR/CNFs nanocomposites were studied via tensile testing. Representative stress−strain curves of the samples are shown in Figure 1 and the average properties and their standard deviations are summarized in Table 1. Figure 1a compares the tensile curves of SBR reinforced with three different

DOI: 10.1021/acsomega.9b01313
ACS Omega 2019, 4, 13189−13199

Table 1. Tensile Properties of SBR and SBR/CNF Nanocomposites

samples	modulus (MPa)	failure strength (MPa)	failure strain
neat SBR	1.67 ± 0.06	3.20 ± 0.71	7.14 ± 1.31
industrial SBR	7.35 ± 0.30	16.10 ± 0.91	4.08 ± 0.25
3% CNF	2.75 ± 0.25	4.18 ± 0.34	5.04 ± 0.55
7% CNF	10.33 ± 1.73	8.06 ± 0.95	7.86 ± 0.88
9% CNF	12.29 ± 2.23	6.16 ± 0.15	2.39 ± 0.39
3% TC-CNF	4.71 ± 0.34	5.86 ± 0.20	4.08 ± 0.24
7% TC-CNF	13.01 ± 1.40	7.43 ± 0.16	3.23 ± 0.16
9% TC-CNF	12.79 ± 1.58	10.32 ± 0.39	2.76 ± 0.14
3% A4-CNF	3.65 ± 0.49	6.30 ± 0.31	5.91 ± 0.98
7% A4-CNF	12.65 ± 3.17	10.49 ± 0.42	2.17 ± 0.36
9% A4-CNF	22.14 ± 2.78	12.77 ± 0.16	1.57 ± 0.16
3% A4-CNF-Tol[a]	4.63 ± 0.23	7.04 ± 0.61	4.21 ± 0.21
7% A4-CNF-Tol[a]	12.00 ± 2.57	11.16 ± 0.46	2.60 ± 0.15
9% A4-CNF-Tol[a]	26.75 ± 3.36	12.26 ± 0.35	1.79 ± 0.16
7% T3-CNF	9.78 ± 1.95	9.03 ± 0.29	3.57 ± 0.48
7% T11-CNF	11.51 ± 1.76	8.66 ± 0.57	2.04 ± 0.30
7% A10-CNF	9.67 ± 1.18	9.37 ± 0.34	3.32 ± 0.12

[a]Nanocomposite samples prepared using toluene as the solvent.

concentrations (i.e., 3, 7, and 9%) of pristine CNFs. The curves for industrial SBR and neat SBR are also shown as the baselines for comparison.

Pristine CNFs provide significant reinforcement to SBR as shown in Figure 1a. Failure strength and elastic modulus of the samples increase with the increasing CNF content up to 7%. The 7% sample shows the best overall results: a modulus increase from 1.64 to 10.33 MPa, a failure strength increase from 3.20 to 8.06 MPa, and a failure strain increase from 714 and 786%. The 9% sample exhibits a further increase in modulus (12.29 MPa) compared with the 7% sample, however, both failure strength (6.16 MPa) and failure strain (239%) of the sample decrease. A decrease in failure strain is typical at high levels of reinforcement loading in polymer composites, which normally suggests significant aggregation of the reinforcement, resulting in formation of defect sites inside the nanocomposites.[9,24] The overall increases in mechanical properties by the CNF reinforcement is attributed to the load sharing of the CNFs from the SBR matrix. The formation of a percolating CNF network is also likely and contributes to the property increases. The increases also suggest that the solution blending process is relatively effective in dispersing hydrophilic pristine CNFs in the hydrophobic SBR matrix.

It is interesting to note the difference in stress−strain behaviors between the industrial SBR (or neat SBR) and the SBR/CNFs nanocomposites: a nearly linear stress−strain relationship at large strains for the former and an extensive yielding and cold drawing process similar to the behavior of thermoplastics for the latter (especially the samples containing 7 and 9% CNFs). Rubber elasticity is entropy driven and rubber deformation does not normally show yielding and cold drawing, which are typical signs of irreversible plastic deformation of materials. Being a covalently linked polymer network, rubber has the ability to undergo large reversible deformation at relatively low stresses. The yielding and cold drawing that occurred on the CNF-reinforced SBR may be partially attributed to interfacial debonding and interfacial slip between CNFs and SBR, which leads to large-scale irreversible deformation. Additionally, the CNFs in SBR during sulfur vulcanization could serve as physical barriers that hindered the reaction and therefore reduced the number of cross-links between rubber chains. If the CNFs can also form covalent links with the rubber chains, it should be expected that the yielding and cold drawing behaviors will be largely mitigated, as will be discussed later.

While pristine CNFs do show a significant reinforcement effect, the material pales in comparison with 50 phr carbon black that is used in industrial SBR, which displays a modulus of 7.35 MPa, a failure strength of 16.10 MPa, and a failure strain of 408%. Carbon black's large influence on the mechanical properties of the rubber stems from both filler−rubber and filler−filler interactions. The filler−rubber interaction can be described as a complex physical−chemical interaction in which carbon black is entangled within a web of rubber chains. Carbon black can then interact with rubber chains via both van der Waals' and covalent interactions depending on the surface reactivity of both rubber chains and carbon black. The number of covalently attached rubber chains to the surface of carbon black increases with decreasing carbon black particle size and increasing particle surface activity.[3,5,27] Above a threshold concentration, homogenously dispersed carbon black nanoparticles tend to form a percolated 3-dimensional network through filler−filler interactions within the matrix elastomer, which also contributes to the reinforcement.

When comparing the reinforcement effect of pristine CNFs and carbon black, it is important to note that CNF loading levels are significantly lower than that of carbon black. The reinforcement potential of CNFs is therefore much higher than that of carbon black as they provide a greater increase per percent of the reinforcing material. For instance, each percent of carbon black and CNFs leads to an 8 and 22% average increase to the failure strength of the rubber (calculated by the percentage strength increase divided by the corresponding filler content), respectively. The higher reinforcing efficiency of CNFs is primarily because of the material's fibrillar shape (i.e., high aspect ratio) and high strength and modulus. Based on composite mechanics theory, other conditions being equal, the reinforcing material with a higher aspect ratio and higher strength and modulus leads to stronger reinforcement to the matrix. CNFs, being nanofibers with exceptional strength and modulus, is therefore much more effective at reinforcing SBR than spherical carbon black particles.

Figure 1b shows the stress−strain curves of the SBR samples reinforced with surface-functionalized CNFs. Five varieties of functionalized CNFs were tested at a loading level of 7% to determine which functionalization method had the greatest effect on the resulting nanocomposite properties. The five functionalization methods introduced either −SH or −C═C functional groups to the surface of the CNFs, as listed in Table 3. Each variant of the functionalized CNFs is shown to provide improvement on the mechanical properties of the resulting SBR nanocomposites over the pristine CNFs. Modulus and failure strength of the nanocomposites increased across the board when the pristine CNFs were replaced with the functionalized CNFs, whereas the fracture strain decreased. These changes can be attributed to the grafted −SH or −C═C groups, through which the functionalized CNFs are covalently linked to the SBR chains during the sulfur vulcanization process. The covalent bonding between SBR and the functionalized CNFs increases stress transfer between the two phases when the composites are under load and

DOI: 10.1021/acsomega.9b01313
ACS Omega 2019, 4, 13189−13199

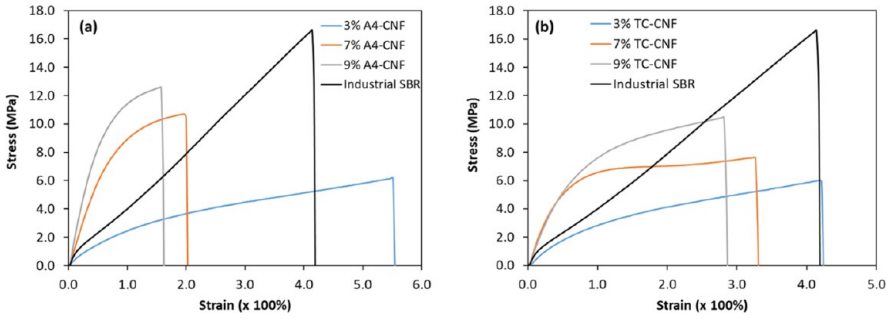

Figure 2. Representative tensile stress−strain curves of SBR reinforced by functionalized CNFs. (a) 4-pentenoic acid-functionalized CNFs and (b) cysteine-functionalized CNFs.

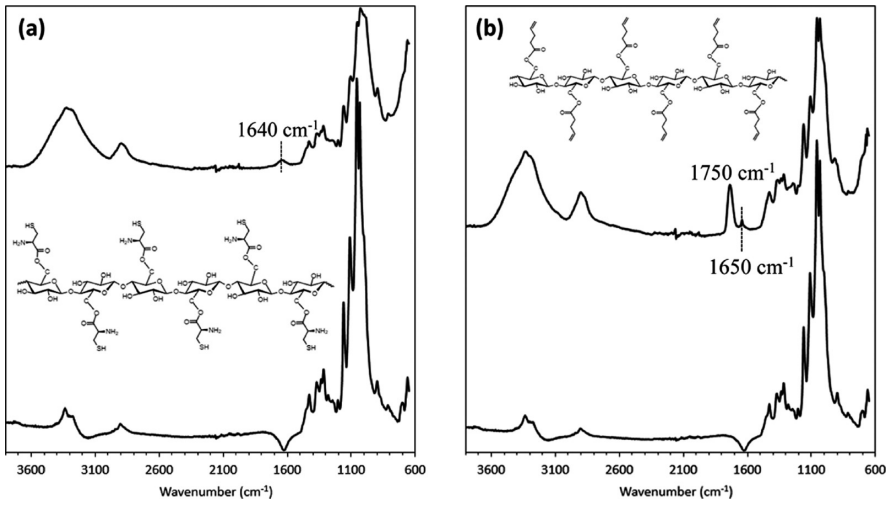

Figure 3. FT-IR spectra of (a) TC-CNF and (b) A4-CNF. The spectrum of the pristine CNFs is shown at the bottom of each figure for comparison.

restricts the mobility of the SBR chains, thus leading to improved reinforcement compared with the pristine CNFs. Also, because of the improved interfacial bonding, the extensive cold drawing process demonstrated by the pristine CNF-reinforced SBR can be seen largely depressed in the SBR samples reinforced by functionalized CNFs (see Figure 1b).

Figure 1b demonstrates that SBR reinforced with functionalized CNFs is one step closer in terms of mechanical properties to the industrial SBR. Among the functionalized CNFs, TC-CNF, T3-CNF, and T11-CNF have the same functional −SH groups on their surfaces. Their effects on the mechanical properties of SBR can be compared using the data (i.e., 7% TC-CNF, 7% T3-CNF, and 7% T11-CNF) given in Table 1. 7% TC-CNF shows the highest modulus but the lowest strength among the three samples; 7% T11-CNF shows a lower modulus and a higher strength compared with 7% TC-CNF; 7% T3-CNF has the lowest modulus but the highest strength among the samples. The different reinforcement results rendered by the three functionalization agents can be related to their different chain lengths (e.g., 11-mercaptoundecanoic acid vs 3-mercaptopropionic acid) and molecular structures (e.g., the additional $-NH_2$ group on cysteine), which can affect the interactions between SBR and the functionalized CNFs and the dispersion of the nanofibers. A similar phenomenon can also be observed from the nanocomposites reinforced by the CNFs functionalized with −C═C groups, that is, 7% A4-CNF and 7% A10-CNF in Table 1. A4-CNF produced a higher composite modulus and strength than A10-CNF. Further studies are needed to understand the steric effects of these different agents on the mechanical properties of the nanocomposites. Below A4-CNF and TC-CNF will be chosen as respective representative for −SH- and −C═C-functionalized CNFs to study their impacts on other properties of SBR at different nanofiber concentrations.

Figure 2 details stress−strain results for the A4-CNF- and TC-CNF-reinforced SBR at 3, 7, and 9% nanofiber concentrations. Both types of nanocomposites show increases in strength and modulus and decreases in failure strain with the increasing nanofiber concentration. For all three concentrations, the functionalized CNFs produce higher modulus and strength than the pristine ones, again due to the increased interfacial bonding between the functionalized CNFs and SBR. The decrease in failure strain can be attributed to increasingly restrained mobility of SBR chains at higher nanofiber concentrations. Comparing Figure 2a,b, A4-CNF is shown to give higher strength and modulus than TC-CNF at the same nanofiber concentrations. These results suggest that the interfacial bonding between A4-CNF and SBR is stronger than that between TC-CNF and SBR, which may be ascribed to a lower density of grafted −SH on the CNF surface, as indicated by the Fourier transform infrared (FTIR) results presented in the next section.

The A4-CNF-reinforced SBR nanocomposites were also prepared using toluene as the solvent. Toluene is less polar than tetrahydrofuran (THF) while A4-CNF is much less hydrophilic compared with the pristine CNF because of the

DOI: 10.1021/acsomega.9b01313
ACS Omega 2019, 4, 13189−13199

grafted hydrocarbon short chains. Therefore, A4-CNF should have a better dispersion in toluene than in THF, which can result in better reinforcement to the rubber. In Table 1, comparing the data for the SBR/A4-CNF nanocomposites prepared using THF and toluene, respectively (e.g., 3% A4-CNF vs 3% A4-CNF-Tol), the samples prepared using toluene generally show comparable or moderately improved mechanical properties, suggesting the polarity of the solvent does have an impact on the nanocomposite properties. However, because the impact is not significant, toluene is not further tested on other nanocomposites.

Cellulose Surface Chemical Analysis. FT-IR spectra of TC-CNF, A4-CNF, and the pristine CNFs are compared in Figure 3. The peak at approximately 1640 cm^{-1} in Figure 3a is associated with the N−H bend of the primary amine present in the cysteine molecules. The presence of this peak indicates the presence of covalently attached cysteine molecules on the surface of TC-CNF. The peak at approximately 1750 cm^{-1} in Figure 3b is associated with the carbonyl group (C═O) present on the ester linkages. The peak at approximately 1650 cm^{-1} is associated with the −C═C groups on the 4-pentenoic acid. The presence of these peaks indicates that the esterification procedures to graft cysteine and 4-pentenoic acid onto CNF surface were successful.

Elemental analysis was performed to further support the FT-IR results. Table 2 details the elemental percentages of C, N, H, S, and O of the pristine and functionalized CNFs. The theoretical composition of the pristine cellulose is also provided for comparison. It is important to note that elemental analysis performed did not yield oxygen percentages. Percent oxygen values listed in Table 2 were calculated assuming that oxygen makes up the remaining mass of each cellulose material.

Table 2. Elemental Analysis Results for the Pristine and Functionalized CNFs

	C (%)	H (%)	N (%)	S (%)	O (%)
pristine CNF (theoretical)	44.45	6.22			49.34
pristine CNF	42.20	5.95			51.85
TC-CNF	41.68	6.09	1.16	2.38	48.69
A4-CNF	46.64	6.57			46.79

The theoretical and experimental compositions of the pristine CNFs are similar, demonstrating the accuracy of this analysis method. For A4-CNF, the degree of substitution (DS) can be estimated according to a previously published method to be approximately 0.15.[28] The formulation for the calculation of DS however does not work in the case where the substitute molecules contain nitrogen and sulfur elements. However, the elemental data can still be used to prove the successful grafting of cysteine onto CNFs. The elements N and S (one of each) of the cysteine molecule should be present in the final TC-CNF in a fashion consistent with the individual molecular weights of N and S present on the cysteine molecule. The molecular weight of N and S is 14.007 and 32.06, respectively. The theoretical mass ratio of N to S of a single cysteine molecule is 0.4369. Elemental analysis found that TC-CNF contained a ratio of N to S of 0.4874. These similar results indicate that the cysteine molecule has been successfully attached to the CNF surface.

Nanocomposite Morphology. Nanocomposite morphologies were studied via scanning electron microscopy (SEM) imaging of cryo-fractured and tensile fractured sample surfaces. Figure 4 shows images of cryo-fractured neat SBR as well as the SBR/pristine CNFs nanocomposites. The surface of the neat SBR is largely smooth and flat, dotted with particles measuring less than 1 μm (Figure 4a,b). The exact identity of these particles is unknown but could be aggregated vulcanization agents or simply impurities. The addition of the pristine CNFs significantly increases the number of the particles present on the sample surfaces, as shown in Figure 4c,e,f. CNFs and their bundles can be clearly seen on the high magnification images on the right. Some relatively large CNF agglomerates are also present, especially in the composites with high CNF contents. In general, the number of the large irregular agglomerates increases with the increasing CNF content. Aggregation of the pristine CNFs at high concentrations is somewhat expected because of the incompatibility between hydrophilic nanofibers and the hydrophobic SBR matrix. However, they still show significant positive effects on SBR mechanical properties, as shown earlier. Specifically, at 7% CNF concentration, strength, modulus, and strain of the nanocomposite are all higher than those of the neat SBR (see Table 1).

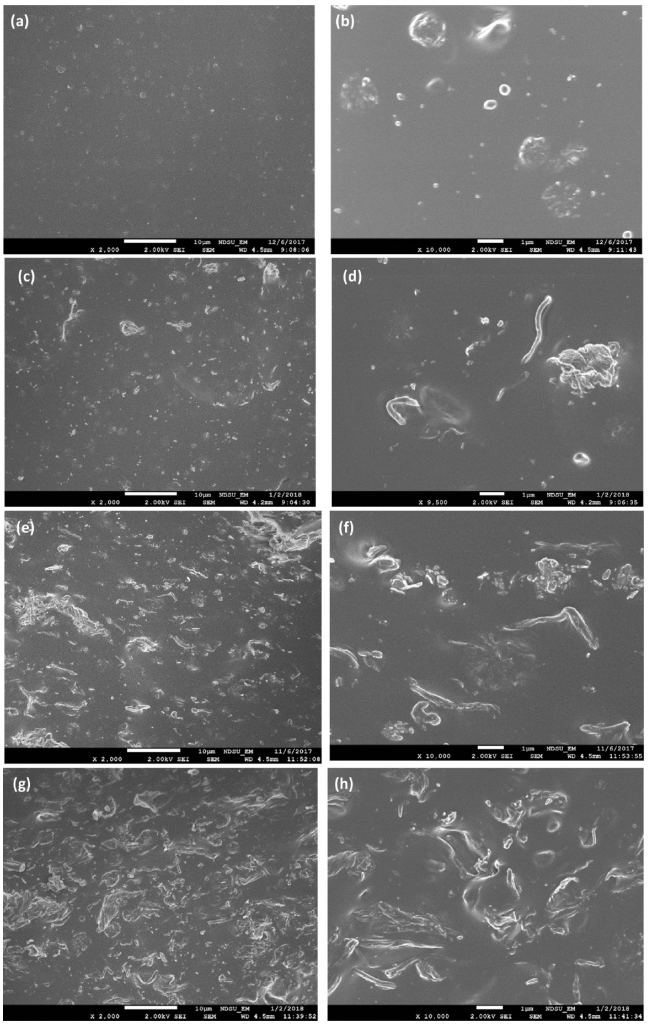

Figure 4. SEM images of cryo-fractured surfaces of neat SBR and SBR/CNFs nanocomposites. (a,b) Neat SBR, (c,d) 3% CNFs, (e,f) 7% CNFs, and (g,h) 9% CNFs. All CNFs are pristine ones.

DOI: 10.1021/acsomega.9b01313
ACS Omega 2019, 4, 13189−13199

Tensile fracture surfaces of neat SBR and pristine CNF-reinforced SBR samples are compared in Figure 5. The neat

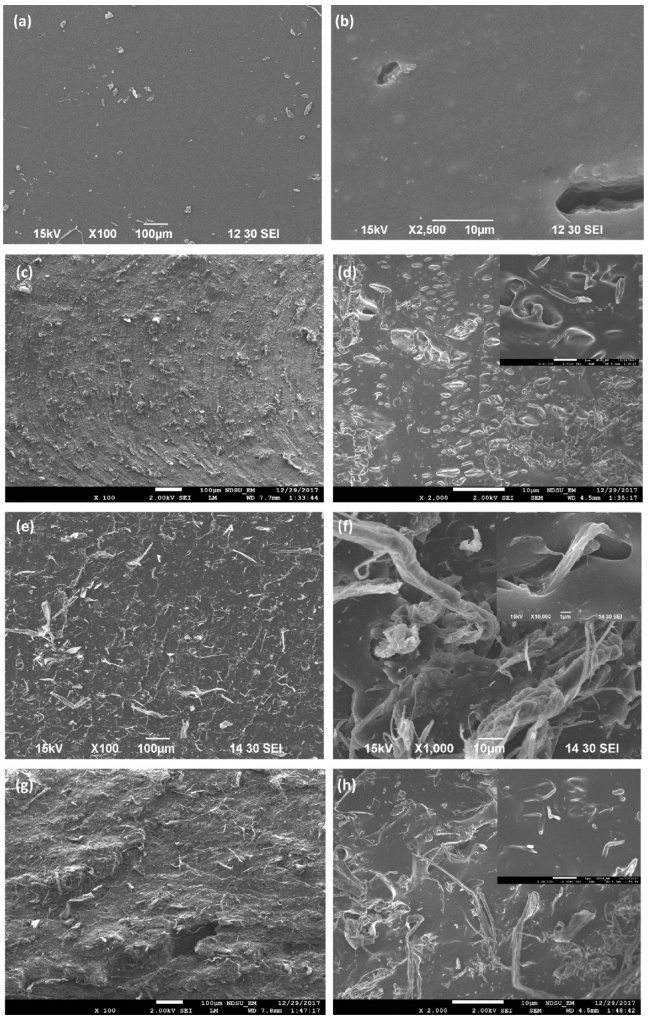

Figure 5. SEM images of tensile fractured surfaces of neat SBR and SBR/CNFs nanocomposites. (a,b) Neat SBR, (c,d) 3% CNFs, (e,f) 7% CNFs, and (g,h) 9% CNFs. All CNFs are pristine ones. Insets are high magnification images.

SBR shows a relatively clean and flat surface decorated by scattered particles (see Figure 5a,b). Some of the particles are embedded on the surface, resembling the structure of the cryo-fractured surface of the neat SBR (Figure 4a,b). Other particles appear to be loosely deposited on the surface. These particles may originate from other regions of the fracture surface; they broke away from the surface and landed at their current locations during the fracture process. The incorporation of various concentrations of the pristine CNFs drastically changed the features of the fracture surfaces (Figure 5c–h). The sample with 3% CNFs clearly shows a much rougher surface compared with the neat SBR. The high roughness can be ascribed to the many voids on the surface that are formed when the particles are pulled out during the tensile test (Figure 5c,d). Further increases in the CNF content result in even rougher surfaces, showing fibers with various sizes being pulled out from the matrix. The fiber pull out indicates that the fiber-matrix interfacial bonding is relatively weak for the pristine CNFs. The presence of large fiber bundles on the surfaces suggests poor compatibility between the pristine CNFs and SBR. Although many large size particles can be seen on these surfaces, high magnification images (insets in Figure 5) clearly show that there are also numerous nanosized cellulose fibers present on the facture surfaces.

The morphology of SBR/A4T-CNF-Tol nanocomposites prepared using toluene is shown in Figure 6. As the content of

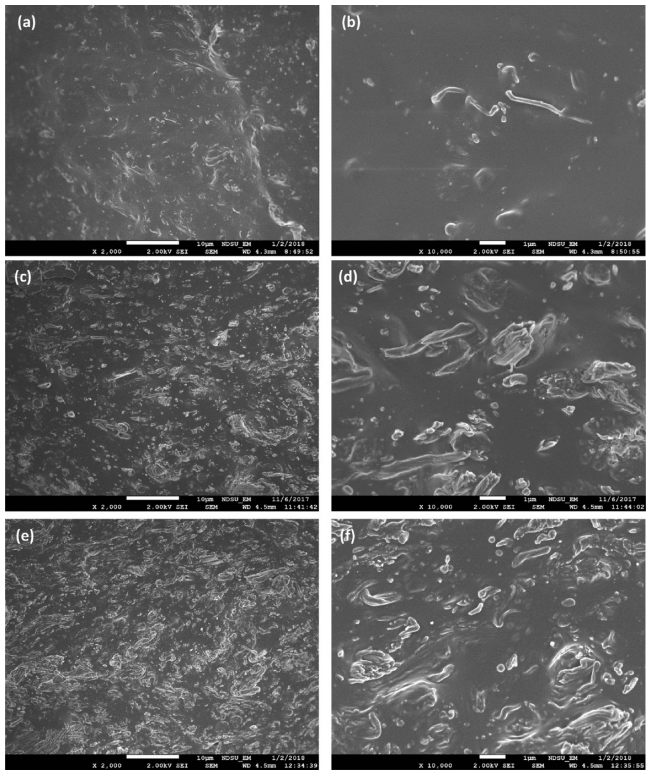

Figure 6. SEM images of cryo-fractured surfaces of SBR/A4-CNF-Tol nanocomposites. (a,b) 3, (c,d) 7, and (e,f) 9%.

A4T-CNF increases, the number of fibers and fiber aggregates on the surfaces also increases, a trend also recognized for the pristine CNFs. However, for A4T-CNF-Tol, the size of the fibers/aggregates is more uniform and is much smaller than that of the pristine CNFs. The smaller and more densely populated fibers/aggregates indicate that the surface-modified A4T-CNF is more uniformly dispersed in the SBR matrix than its pristine counterpart because of its increased compatibility with the rubber matrix. This better dispersion, together with the chemical linkage established between the fiber and the rubber during vulcanization, led to the improved mechanical properties of the A4-CNF-reinforced SBR nanocomposites.

SEM images of the tensile-fractured SBR/A4T-CNF-Tol nanocomposites are shown in Figure 7. The surfaces appear to be similar to those of the SBR/pristine CNFs nanocomposites (Figure 5): high roughness, voids, and pulled-out fibers. However, a close comparison between the two materials indicates that the composites containing the pristine CNFs do show more severe fiber pull-out and more signs of matrix deformation than those containing the functionalized CNFs, in agreement with the tensile results that the former exhibits lower failure strength but higher failure strain than the latter (see Table 1). For comparison, the tensile fracture surfaces of SBR/TC-CNF nanocomposites are also shown in Figure 8. The surfaces appear similar to those of SBR/A4T-CNF-Tol. A subtle difference is that SBR/TC-CNF does show more

DOI: 10.1021/acsomega.9b01313
ACS Omega 2019, 4, 13189−13199

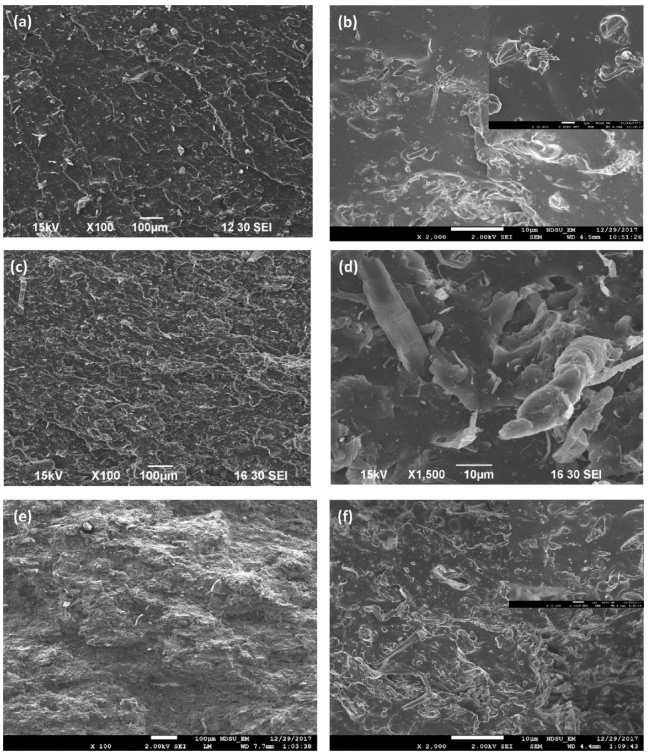

Figure 7. SEM images of tensile-fractured surfaces of SBR/A4-CNF-Tol nanocomposites. (a,b) 3, (c,d) 7, and (e,f) 9%. Insets are high magnification images.

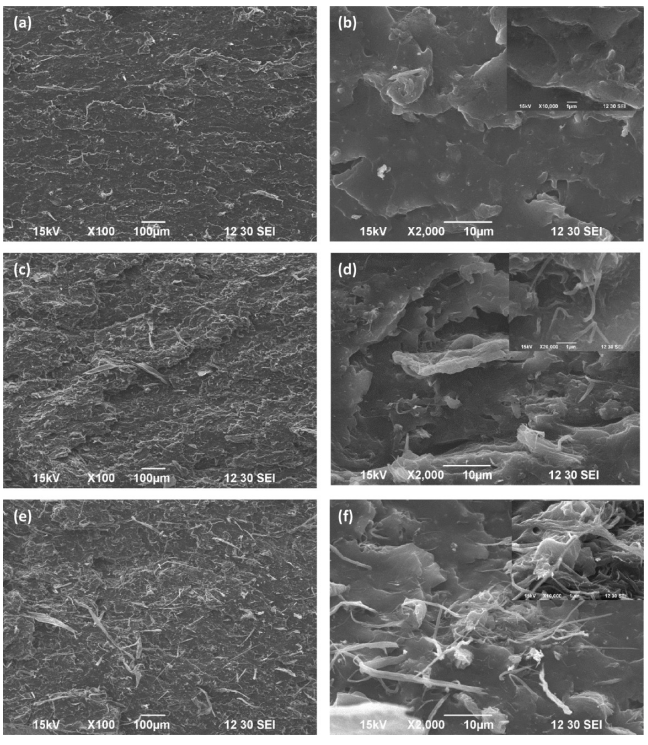

Figure 8. SEM images of tensile-fractured surfaces of SBR/TC-CNF nanocomposites. (a,b) 3, (c,d) 7, and (e,f) 9%. Insets are high magnification images.

material deformation and fiber pull-out. This behavior is typically associated with more ductile nanocomposite behavior and agrees well with the tensile results as the SBR/TC-CNF nanocomposites have a higher fracture strain compared to the SBR/A4T-CNF samples. This result combined with the fact that the TC-CNF nanocomposites displayed a lower failure strength than the A4T-CNF ones suggests that the fiber-matrix interactions in SBR/TC-CNF is weaker than that in SBR/A4T-CNF.

Viscoelastic Properties. Tan δ is an important parameter to characterize damping of rubber products. A lower tan δ indicates an increase in rigidity of a material and its lower capability to dissipate energy. The tan δ curves for the neat rubber and its various nanocomposites are compared in Figure 9. The pristine CNFs reduced tan δ of SBR, with a higher nanofiber concentration leading to a larger decrease (see Figure 9a). The functionalized CNFs, shown in both Figure 9b,c, appear to cause even larger decreases in tan δ (especially in the case of A4T-CNF), indicating their stronger restraints to SBR chain mobility than the pristine CNFs. It is interesting to note that the tan δ peak temperature for SBR/A4T-CNF-Tol nanocomposites decreases with increasing nanofiber content (Figure 9b). The peak is associated with the glass transition of SBR. The decrease in the peak temperature for these samples may be attributed to the toluene solvent used in preparing the nanocomposites. Toluene has a much higher boiling point than THF (110 vs 66 °C) and it is possible that some toluene remained in the composites after the sample preparation process. The residual toluene in the SBR/A4T-CNF-Tol nanocomposites functioned as a plasticizer to lower the glass transition temperature of SBR. By contrast, THF used for preparing the other two nanocomposites was mostly removed during the preparation process because of its low boiling point. Therefore, TC-CNF slightly increased the glass transition temperature of SBR because of its strong restraint on chain mobility (Figure 9c), whereas the pristine CNFs showed a negligible effect on the glass transition (Figure 9a).

Solvent Resistance. SBR dissolves in toluene if not vulcanized. Vulcanization covalently links SBR chains together to form a network and therefore the vulcanized SBR only swells, rather than dissolve, in toluene. Other conditions being equal, solvent absorbancy of the rubber is inversely proportional to the degree of cross-linking. Additionally, CNFs (pristine and functionalized alike) also affect solvent absorbency because it can slow down solvent diffusion in the rubber and restrain chain movement to reduce swelling. Studying the solvent intake of the SBR/CNFs nanocomposites can produce information regarding their cross-linking status and morphology. Figure 10 shows toluene absorbency as a function of time for the neat SBR and its nanocomposites. In general, all the samples exhibit a similar absorption pattern in which the rate of absorption (slope of the curve) is high initially but decreases gradually over the 80 min soaking time. The incorporation of both pristine and functionalized CNFs decreased the absorbency and the rate of absorption of the samples, with a higher CNF content leading to a larger decrease in both properties. This result confirms the nanofibers' hindrance to solvent diffusion and rubber chain movement, especially at high nanofiber concentrations when a nanofiber network may form inside the rubber. The barrier effect of the CNFs can be particularly strong in the CNF-rich regions of the nanocomposites, where SBR chains can be trapped by the nanofibers and hence have no access to the solvent.

There is a notable difference in toluene uptake between the pristine CNFs and the functionalized CNF-reinforced SBR. As

DOI: 10.1021/acsomega.9b01313
ACS Omega 2019, 4, 13189−13199

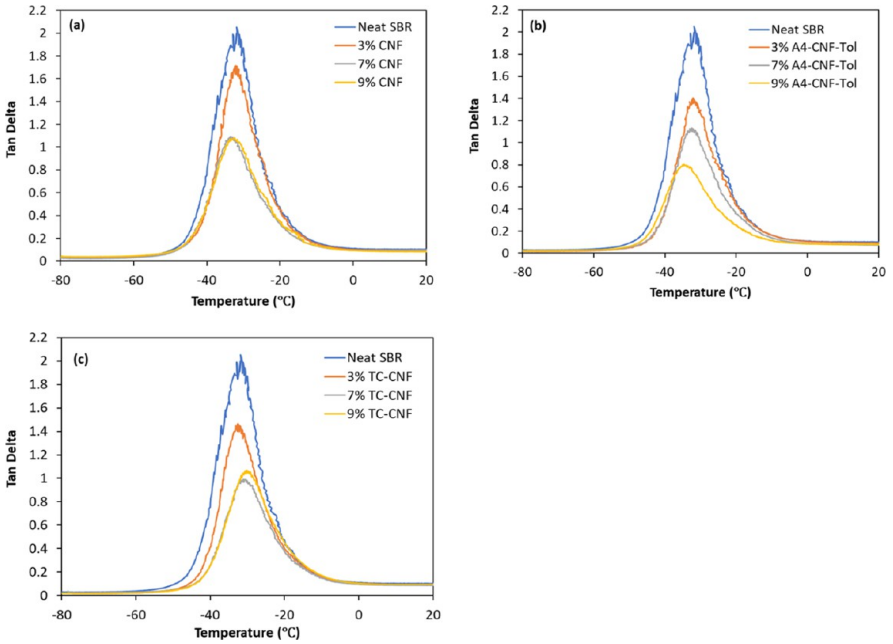

Figure 9. Tan δ of (a) SBR/pristine CNF, (b) SBR/A4T-CNF-Tol, and (c) SBR/TC-CNF nanocomposites.

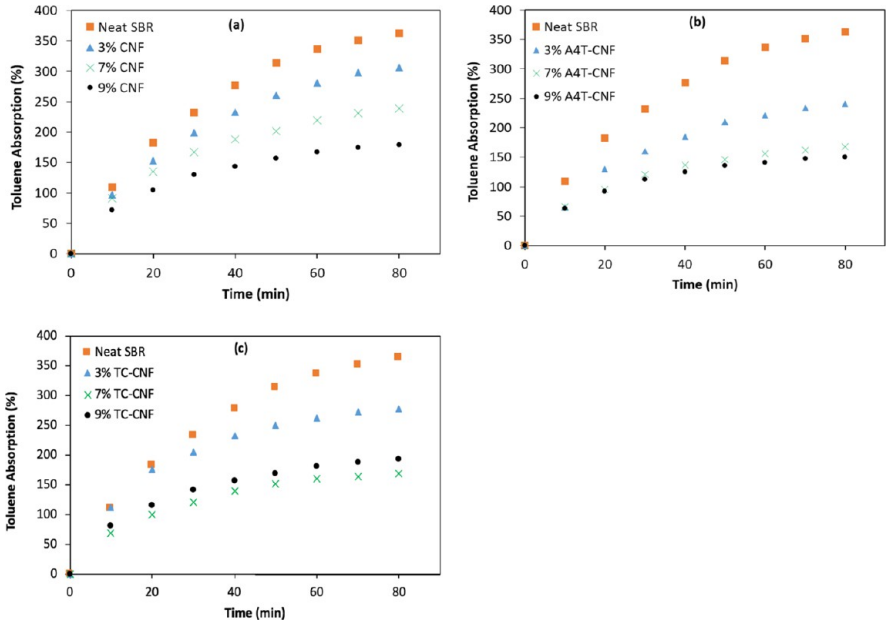

Figure 10. Toluene uptake of (a) SBR/pristine CNFs, (b) SBR/A4T-CNF-Tol, and (c) SBR/TC-CNF nanocomposites.

shown in the SEM results earlier, the functionalized CNFs exhibit more uniform dispersion in SBR and show a smaller average particle size than the pristine CNFs. This leads to a larger volume of interphase regions in the nanocomposites where the movement of SBR chains is restrained by the nanofibers. The functionalized CNFs also exert a higher level of restraints on the surrounding SBR chains than the pristine CNFs because of the former's covalent bonds to the chains. These two factors together contribute to the lower toluene uptake of the SBR reinforced with functionalized CNFs. Comparing the uptakes between the SBR/A4-CNF-Tol and the SBR/TC-CNF nanocomposites (Figure 10b,c), the former shows a lower uptake after the same period of immersion time, with the difference being particularly large for the two nanocomposites containing 3% nanofibers. This can be attributed to A4-CNT's better dispersion in SBR because of the use of toluene as the solvent. The improved dispersion also contributes to the higher mechanical properties of the SBR/A4-CNF-Tol nanocomposites, as discussed earlier in the mechanical properties section.

CONCLUSIONS

In this study, industrially important SBR was reinforced with pristine and functionalized CNFs. The functionalization of CNFs was performed through the esterification reaction using five different reagents and as a result, −SH or −C═C functional groups were successfully attached to the nanofiber surface. Mechanical testing showed that CNFs (pristine or functionalized alike) showed much higher reinforcement

DOI: 10.1021/acsomega.9b01313
ACS Omega 2019, 4, 13189−13199

efficiency than carbon black, an industrial standard filler material. All the functionalized CNFs demonstrated stronger reinforcement than the pristine CNFs because of the former's better dispersion in the SBR matrix and covalent bonding with the rubber chains. Damping of all the rubber nanocomposites was reduced, with the functionalized CNFs causing larger decreases because of their larger surface areas (better dispersion) and stronger restraints on chain mobility than the pristine CNFs. Solvent resistance of the rubber was also improved after incorporating CNFs because of the barrier effect of the nanofibers and the restrained chain movement.

Although CNFs, especially functionalized CNFs, can lead to higher SBR strength and modulus than carbon black at the same filler concentration, the decrease in damping may not be desired for some applications. Additionally, properties such as UV resistance and conductivity that are rendered by carbon black are also lost in the carbon black-free SBR. A logical next step is to develop CNFs/carbon black/SBR hybrid nanocomposites, in which performance synergy may originate from the two reinforcements. This new development will be reported in our forthcoming publication.

EXPERIMENTAL SECTION

Materials. CNFs were purchased from the Process Development Center of University of Maine. SBR (KER 1502 SBR) was supplied by Synthos S.A. N330 grade carbon black was acquired from Sid Richardson Carbon & Energy Co. Sulfur, *N-tert*-butyl-2-benzothiazyl sulfonamide (TBBS), stearic acid, zinc oxide, 1-ethyl-3-(3-dimethylaminopropyl)-carbodiimide (EDC), 4-dimethylaminopyridine (DMAP), 4-pentenoic acid, 10-undecenoic acid, 3-mercaptopropionic acid, 11-mercaptoundecanoic acid, cysteine, THF, anhydrous dimethylformamide (DMF), and sodium hydroxide (NaOH) were of reagent grade and purchased from Sigma-Aldrich.

Preparation of Surface-Functionalized CNFs. CNFs were esterified using a one-step Steglich esterification technique typically utilized for protein and peptide modification. CNFs were first solvent exchanged via centrifugation into anhydrous DMF. The resulting suspension was then added to a round-bottomed flask. Additional anhydrous DMF was added at a CNFs/DMF ratio of 1:100 (g/mL). EDC and DMAP were then added in excess to the suspension at the same CNFs/reagent ratio of 1.25:1 (g/g). 0.45 mM of various functional reagents specified in Table 3 were then added to the suspension. The round-bottomed flask was then stirred for 24 h at room temperature. The resulting esterified CNFs were then washed to remove residual chemicals in THF, deionized (DI) water and/or toluene via centrifugation.

Table 3. Reagents for CNF Functionalization and the Designations of the Functionalized CNFs

designation	functional reagent	functional group
T3-CNF	3-mercaptopropionic acid	mercapto (−SH)
T11-CNF	11-mercaptoundecanoic acid	mercapto (−SH)
A4-CNF	4-pentenoic acid	vinyl (−C═C)
A10-CNF	10-undecenoic acid	vinyl (−C═C)
TC-CNF	cysteine	mercapto/amine (−SH/−NH_2)

Steglich esterification is a mild reaction in which dicyclohexylcarbodiimide (DCC) is typically used as a coupling reagent and DMAP as a catalyst to allow ester formation from alcohols and carboxylic acids.[29] In this work, EDC is substituted for DCC to avoid the formation of dycyclohexylurea, which is poorly soluble in water.[30] EDC and DCC share the same coupling mechanism. However, the byproduct from EDC coupling is isourea, which is soluble in water. Water solubility of the byproduct allows for easy extraction via centrifugation.

Preparation of Vulcanized SBR Nanocomposites. An industrial SBR formulation used by Nocil Limited was chosen as the base formulation. The base formulation (industrial SBR) and the formulations for SBR/CNFs nanocomposites are given in Table 4. The industrial SBR was incorporated with 50 phr carbon black. The SBR/CNFs nanocomposites contained at 3, 7, or 9 wt % CNFs based on the SBR weight. Neat SBR containing no carbon black was also prepared for property comparison.

Table 4. Formulations for SBR and SBR/CNFs Nanocomposites Investigated in This Study

material	neat SBR (phr)	industrial SBR (phr)	SBR/CNFs (phr)
SBR	100	100	100
sulfur	1.75	1.75	1.75
zinc oxide	3	3	3
stearic Acid	1	1	1
TBBS	1	1	1
carbon black	0	50	0
CNFs	0	0	3.09 (3%), 7.53 (7%), or 9.89 (9%)

The industrial SBR samples were prepared using a standard rubber compounding procedure. The ingredients listed in Table 4 were loaded into a HAAKE RHEOMIX OS lab mixer, equipped with Banbury-type mixing blades and a chamber volume of 60 ccm. Samples were kneaded at 20 rpm until the torque output from the lab mixer stabilized. This usually took approximately 7−9 min. The temperature of the mixing chamber was set to 60 °C and allowed to increase to approximately 70 °C during operation. Samples were then shaped into disks using a Brabender Prep-Mill laboratory two-roll mill with a roller temperature of 60 °C. Shaped rubber disks were then vulcanized via pressing in an Elcometer heated press at 2400 N and 145 °C for 36 min. The neat SBR samples were prepared following the same procedure except without incorporating any carbon black.

SBR/CNFs nanocomposites were prepared by first using a solution casting technique to incorporate pristine CNFs or the functionalized CNFs into SBR. SBR gum rubber was dissolved in THF at room temperature. Vulcanization reagents and CNFs were then added to the solution and the suspension was homogenized using an ULTRA-TURRAX homogenizer (IKA, Wilmington, NC, USA) equipped with IKA 25N 25F dispersing elements (6000 rpm) for 15 min. The homogenized suspension was then dried by natural evaporation at room temperature followed by drying in a vacuum oven for 12 h. The dried samples were further blended and shaped into disks using a Brabender Prep-Mill laboratory two-roll mill with a roller temperature of 60 °C. The shaped rubber disks were then vulcanized via pressing in an Elcometer hot press under 2400 N and 145 °C for 36 min.

DOI: 10.1021/acsomega.9b01313
ACS Omega 2019, 4, 13189−13199

To examine the effect of the solvent on the mechanical properties of the nanocomposites, toluene was also tested as the solvent in the solution casting process for one nanocomposite (SBR/A4-CNF). Toluene was chosen for this test because of its lower polarity than THF, which may lead to better dispersion of A4-CNF in the SBR matrix.

Tensile Testing. Tensile properties were examined in accordance with ASTM D412-15a. Vulcanized rubber disks were cut into dumbbell shapes using an ASTM D412 certified cutter. A minimum of three samples for each formulation were tested using an MTS Insight electromechanical tester (Eden Prairie, MN, USA) equipped with a 5 kN load cell and Advantage pneumatic grips with rubber-coated surfaces. All tests were conducted under 50% relative humidity and 22 °C temperature with a crosshead speed of 500 mm/min. The test results for each formulation were averaged and a standard deviation was calculated.

Fourier Transform Infrared Spectroscopy. FT-IR was utilized to study and confirm chemical structure changes imparted to the cellulose via surface esterification. A Nicolet 8700 (Thermo Scientific, Waltham, MA, USA) FT-IR equipped with a smart iTR attenuated total reflection module was used to obtain each spectrum. FT-IR spectra were obtained in the range of 4000−650 cm^{-1}.

Elemental Analysis. Elemental analysis was performed by Atlantic Microlab, Inc. (Norcross, GA). Functionalized and pristine CNFs were washed and dried at 60 °C for 8 h in a vacuum oven. CHNS analysis was then performed and the resulting mass percentages of elements C, H, N, and S were obtained.

Scanning Electron Microscopy. Morphology of tensile fracture surfaces were studied using a JEOL JSM-6490LV SEM (JEOL USA, Peabody MA, USA) operating at a 15 kV accelerating voltage. The samples were mounted on the sample stage using colloidal silver paste (Structure Probe Inc., West Chester PA, USA) and coated with gold using a Cressington 108 auto sputter coater (Ted Pella Inc., Redding CA, USA). Samples were also fractured in liquid nitrogen to avoid sample deformation so that the original phase morphology of the samples was retained. The cryo-fractured surfaces were similarly studied using the SEM.

Dynamic Mechanical Analysis. Dynamic mechanical analysis (DMA) experiments were performed using a TA Instruments (New Castle, DE, USA) Q800 DMA operating in the tension mode. A frequency of 1 Hz and a temperature sweep from −80 to 60 °C at 3 °C/min were utilized to study the viscoelastic behavior of the samples as a function of temperature.

Toluene Uptake. Samples were cut into 1 cm × 0.5 cm × 1.4 cm pieces and immersed in toluene at room temperature to study their solvent resistance. Weight increases were recorded every 10 min up to 80 min of total soaking time. Samples were removed from the toluene and lightly dabbed to remove excess solvent. Sample weight was measured using an analytical balance, followed by reimmersion. Toluene uptake at each respective time was calculated as

$$W_{uptake} = [(W_t - W_0)/W_0] \times 100\%$$

where W_0 is the sample initial mass and W_t is the sample mass at immersion time t.

AUTHOR INFORMATION

Corresponding Authors

*E-mail: mohiuddin.quadir@ndsu.edu (M.Q.).
*E-mail: Long.Jiang@ndsu.edu (L.J.).

ORCID

Mohiuddin Quadir: 0000-0003-2811-773X
Long Jiang: 0000-0002-1781-134X

Notes

The authors declare no competing financial interest.

ACKNOWLEDGMENTS

The authors thank North Dakota Soybean Council for its financial support. We are also grateful for material testing and imaging assistance provided by Dr. Chunju Gu of the NDSU Department of Coatings and Polymeric Materials, Gregory Strommen of the NDSU Center for Nanoscale Science and Engineering, and Scott Payne of the NDSU Microscopy Center. Gratitude is also expressed for the support of the NDSU Department of Mechanical Engineering and many of its staff members.

REFERENCES

(1) Zhang, Y.; Ge, S.; Tang, B.; Koga, T.; Rafailovich, M. H.; Sokolov, J. C.; Peiffer, D. G.; Li, Z.; Dias, A. J.; McElrath, K. O.; Lin, M. Y.; Satija, S. K.; Urquhart, S. G.; Ade, H.; Nguyen, D. Effect of carbon black and silica fillers in elastomer blends. *Macromolecules* **2001**, *34*, 7056−7065.

(2) Wang, M.-J. Effect of polymer-filler and filler-filler interactions on dynamic properties of filled vulcanizates. *Rubber Chem. Technol.* **1998**, *71*, 520−589.

(3) Stearns, R. S.; Johnson, B. L. Interaction between carbon black and polymer in cured elastomers. *Ind. Eng. Chem.* **1951**, *43*, 146−154.

(4) Ciesielski, A., *An Introduction to Rubber Technology*. iSmithers Rapra Publishing, 1999.

(5) Spahr, M. E.; Rothon, R. Carbon Black as a Polymer Filler. In *Polymers and Polymeric Composites: A Reference Series*; Palsule, S., Ed.; Springer Berlin Heidelberg: Berlin, 2016; pp 1−31.

(6) Sae-Oui, P.; Thepsuwan, U.; Thaptong, P.; Sirisinha, C. Comparison of reinforcing efficiency of carbon black, conductive carbon black, and carbon nanotube in natural rubber. *Adv. Polym. Technol.* **2014**, *33*, 21422.

(7) Praveen, S.; Chattopadhyay, P. K.; Albert, P.; Dalvi, V. G.; Chakraborty, B. C.; Chattopadhyay, S. Synergistic effect of carbon black and nanoclay fillers in styrene butadiene rubber matrix: development of dual structure. *Composites, Part A* **2009**, *40*, 309−316.

(8) Mao, Y.; Wen, S.; Chen, Y.; Zhang, F.; Panine, P.; Chan, T. W.; Zhang, L.; Liang, Y.; Liu, L. High performance graphene oxide based rubber composites. *Sci. Rep.* **2013**, *3*, 2508.

(9) Trovatti, E.; Carvalho, A. J. F.; Ribeiro, S. J. L.; Gandini, A. Simple green approach to reinforce natural rubber with bacterial cellulose nanofibers. *Biomacromolecules* **2013**, *14*, 2667−2674.

(10) Mariano, M.; El Kissi, N.; Dufresne, A. Cellulose nanocrystal reinforced oxidized natural rubber nanocomposites. *Carbohydr. Polym.* **2016**, *137*, 174−183.

(11) Xing, W.; Tang, M.; Wu, J.; Huang, G.; Li, H.; Lei, Z.; Fu, X.; Li, H. Multifunctional properties of graphene/rubber nanocomposites fabricated by a modified latex compounding method. *Compos. Sci. Technol.* **2014**, *99*, 67−74.

(12) Xing, W.; Li, H.; Huang, G.; Cai, L.-H.; Wu, J. Graphene oxide induced crosslinking and reinforcement of elastomers. *Compos. Sci. Technol.* **2017**, *144*, 223−229.

(13) Tang, M.; Xing, W.; Wu, J.; Huang, G.; Xiang, K.; Guo, L.; Li, G. Graphene as a prominent antioxidant for diolefin elastomers. *J. Mater. Chem. A* **2015**, *3*, 5942−5948.

DOI: 10.1021/acsomega.9b01313
ACS Omega 2019, 4, 13189−13199

(14) Moon, R. J.; Martini, A.; Nairn, J.; Simonsen, J.; Youngblood, J. Cellulose nanomaterials review: structure, properties and nanocomposites. *Chem. Soc. Rev.* **2011**, *40*, 3941−3994.
(15) Kalia, S.; Dufresne, A.; Cherian, B. M.; Kaith, B.; Avérous, L.; Njuguna, J.; Nassiopoulos, E. Cellulose-based bio-and nanocomposites: a review. *Int. J. Polym. Sci.* **2011**, *2011*, 1−35.
(16) Visakh, P. M.; Thomas, S.; Oksman, K.; Mathew, A. P. Crosslinked natural rubber nanocomposites reinforced with cellulose whiskers isolated from bamboo waste: Processing and mechanical/thermal properties. *Composites, Part A* **2012**, *43*, 735−741.
(17) Yin, B.; Li, G.; Wang, D.; Wang, L.; Wang, J.; Jia, H.; Ding, L.; Sun, D. Enhanced mechanical properties of styrene−butadiene rubber with low content of bacterial cellulose nanowhiskers. *Adv. Polym. Technol.* **2018**, *37*, 1323−1334.
(18) Chen, Y.; Li, G.; Yin, Q.; Jia, H.; Ji, Q.; Wang, L.; Wang, D.; Yin, B. Stimuli-responsive polymer nanocomposites based on styrene-butadiene rubber and bacterial cellulose whiskers. *Polym. Adv. Technol.* **2018**, *29*, 1507−1517.
(19) Tian, M.; Zhen, X.; Wang, Z.; Zou, H.; Zhang, L.; Ning, N. Bioderived Rubber-Cellulose Nanocrystal Composites with Tunable Water-Responsive Adaptive Mechanical Behavior. *ACS Appl. Mater. Interfaces* **2017**, *9*, 6482−6487.
(20) Rojas, O. J. *Cellulose Chemistry and Properties: Fibers, Nanocelluloses and Advanced Materials*; Springer International Publishing, 2016; Vol. *271*.
(21) Dufresne, A. *Nanocellulose: From Nature to High Performance Tailored Materials*; De Gruyter, 2012.
(22) Parambath Kanoth, B.; Claudino, M.; Johansson, M.; Berglund, L. A.; Zhou, Q. Biocomposites from Natural Rubber: Synergistic Effects of Functionalized Cellulose Nanocrystals as Both Reinforcing and Cross-Linking Agents via Free-Radical Thiol−ene Chemistry. *ACS Appl. Mater. Interfaces* **2015**, *7*, 16303−16310.
(23) Kato, H.; Nakatsubo, F.; Abe, K.; Yano, H. Crosslinking via sulfur vulcanization of natural rubber and cellulose nanofibers incorporating unsaturated fatty acids. *RSC Adv.* **2015**, *5*, 29814−29819.
(24) Rosilo, H.; Kontturi, E.; Seitsonen, J.; Kolehmainen, E.; Ikkala, O. Transition to Reinforced State by Percolating Domains of Intercalated Brush-Modified Cellulose Nanocrystals and Poly(butadiene) in Cross-Linked Composites Based on Thiol−ene Click Chemistry. *Biomacromolecules* **2013**, *14*, 1547−1554.
(25) Chen, M.-L.; Ma, H.-J.; Zhang, S.-Q.; Wang, J.-H. Mercury speciation with L-cysteine functionalized cellulose fibre as adsorbent by atomic fluorescence spectrometry. *J. Anal. At. Spectrom.* **2011**, *26*, 613−617.
(26) Editors of Encyclopaedia Britannica. Styrene-Butadiene Rubber (SBR). *Encyclopedia Britannica*; Encyclopædia Britannica, Inc., 2009.
(27) Karásek, L.; Sumita, M. Characterization of dispersion state of filler and polymer-filler interactions in rubber-carbon black composites. *J. Mater. Sci.* **1996**, *31*, 281−289.
(28) Vaca-Garcia, C.; Borredon, M. E.; Gaseta, A. Determination of the degree of substitution (DS) of mixed cellulose esters by elemental analysis. *Cellulose* **2001**, *8*, 225−231.
(29) Neises, B.; Steglich, W. Simple Method for the Esterification of Carboxylic Acids. *Angew. Chem., Int. Ed. Engl.* **1978**, *17*, 522−524.
(30) Williams, A.; Ibrahim, I. T. A new mechanism involving cyclic tautomers for the reaction with nucleophiles of the water-soluble peptide coupling reagent 1-ethyl-3-(3'-(dimethylamino)propyl)-carbodiimide (EDC). *J. Am. Chem. Soc.* **1981**, *103*, 7090−7095.

DOI: 10.1021/acsomega.9b01313
ACS Omega 2019, 4, 13189−13199